Highly sensitive alkane odour sensors based on functionalised gold nanoparticles

Hadi AlQahtani[a,b*], Mark Sugden[a], Delia Puzzovio[a], Lee Hague[a], Nic Mullin[a], Tim Richardson[a], Martin Grell[a]

[a]Department of Physics and Astronomy, University of Sheffield, Hounsfield Road, Sheffield S3 7RH, UK.

[b]Department of Physics, College of Teachers, King Saud University, Riyadh 11451, Saudi Arabia.

[* corresponding author at: Department of Physics an Astronomy, University of Sheffield, Sehffield, S3 7RH, UK. Tel: +44(0)114 22 23508, Fax: +44 (0)114 22 23555 Email address: Php08hra@sheffield.ac.uk]

Abstract

We deposit dense, ordered, thin films of Au- dodecanethiol core/shell nanoparticles by the Langmuir- Schäfer (LS) printing method, and find that their resistance at ambient temperature responds selectively and sensitively to alkane odours. Response is a rapid resistance increase due to swelling, and is strongest for alkane odours where the alkane chain is similar in length to the dodecane shell. For decane odours, we find a response to concentrations as low as 15 ppm, about 600 times below the lower explosive limit. Response is weaker, but still significant, to aromatic odours (e.g. Toluene, Xylene), while potential interferants such as polar and/or hydrogen- bonding odours (e.g. alcohols, ketones, water vapour) are somewhat rejected. Resistance is weakly dependent on temperature, and recovers rapidly and completely to its original value within the error margin of measurement.

Keywords: Gold nanoparticles sensors, Alkane swelling, Alkane detection, Langmuir-Schäfer.

1. Introduction

Alkanes are commonly used as fuels, e.g. liquid alkanes such as octane and decane are present in petrol, and methane is the largest component in natural gas. Due to their flammable nature, petrol vapours and gas leaks represent considerable explosion hazards, and have caused severe accidents in the domestic sphere [1], the petrol supply chain [2], gas production plants [3] and in mining [4]. These dangers call for an early- warning technology. However, detection with chemical sensors of alkanes below their 'lower explosive limit' (LEL) concentrations is difficult, because due to their chemical nature, alkanes carry no dipoles, do not engage in hydrogen bonding, and do not act as acids or bases. Previous studies on alkane detection used chemoresistive materials that catalyse the oxidative dehydrogenation of light alkanes (methane to butane) [5-8]. Sensing devices based on these materials showed a good response to concentrations well below the alarm limits (10^2 ppm vs. LELs of 10^3 ppm). However, chemoresistive sensors need relatively high working temperatures (300-600 °C), and are particularly sensitive to interference e.g. from humidity and ethanol, both of which often are present in the relevant environments. A practical sensor would therefore require prior filtration [9].

Alternatively, a new approach based on the use of alkanethiol encapsulated gold nanoparticles as chemiresistor sensors was introduced by Wohltjen and Snow in 1998 [10]. They have proposed a physical, rather than chemical, approach to the sensing of combustible odours. Inspired by Wohltjen and Snow, Ahn and co-workers [11] exposed films of ω-(3-thienyl)alkanethiol-gold core/shell nanoparticles to several combustible odours, and found an increase in resistance due to swelling of the films in the odour. Longer ligands led to more sensitive sensors. However, such films were not selective for alkanes, but responded to a range of solvent odours in the order toluene > chloroform > hexane > ethanol, with ethanol still giving a considerable response. From the reported data, it is also not clear if such sensors will be useful for the monitoring of alkane odours as explosion hazards, as the lowest investigated odour concentration of hexane still was 10,000 ppm, dangerously close to the LEL of about 12000 ppm (see table 1).

In a recent work [12], it was also shown that the chain length of alkanethiol affects the electrical resistance response sensitivity to non-polar organic vapours. The longer the chain the higher the response is as the gold nanoparticle films swell more.

Encouraged by the work of Ahn *et al.*, we have tailored gold core/shell nanoparticle (Au-CSNP) films for sensitive and selective response to alkane odours. Instead of ω-(3-thienyl)alkanethiol ligands, we used dodecanethiol ligands without the terminal thiophene ring. Such ligands are expected to be most compatible with similarly apolar alkane odours, but to reject more polar or hydrogen- bonding odours. Also, rather than spincasting [11], we processed core/shell nanoparticles by the Langmuir-Schäfer (LS) printing method [13]. The LS printing allows the formation of dense, highly ordered monolayer films on a water surface prior to transferring films to the solid substrate, while still avoiding the coalescence and fusing of neighbouring gold particles. We therefore suggest that the main transport mechanism in core-shell nanoparticle films is based on quantum mechanical site- to- site tunnelling, and therefore the conductivity (σ) may be described by eq. (1.1) [14-15]:

$$\sigma \propto \exp\left[-\left(2d\beta + \frac{E_C}{kT}\right)\right] \qquad (1.1)$$

where d is the distance between two adjacent cores, β is a tunnelling factor, k is Boltzmann's constant, T is the temperature, and E_C is an activation energy, $E_c \approx e^2/4\pi\varepsilon_r\varepsilon_o r$, wherein r is the radius of the cores, and ε_r is the dielectric constant of the medium separating the cores. Eq. (1.1) thus predicts a response of CSNP film conductivity to swelling, as d and ε_r will change. Note, however, that eq.1 suggests that conductivity is independent of the applied electric field, E, thus implying ohmic I/V behaviour. Terrill *et al.* [16] confirmed ohmic behaviour of several gold clusters stabilised by alkanethiols (octane-, dodecane- or hexadecanethiol) for small fields (up to 20 kV/cm); for larger fields, the I/V characteristics changes to non-linear relationship. Eq. (1.1) is thus the appropriate approximation for small fields, the reader may refer to ref. [17] for a detailed discussion of transport mechanisms in gold nanoparticle films.

2. Experimental Methods

2.1. Au CSNP film fabrication: a glass substrate with a size of (1.5×2)cm^2 was cleaned and sonicated with a warm Helmanex solution for 10 min and then sonicated in a warm IPA for another 10 min. After that, gold contacts, a size of 1mm×2mm and 50 nm thickness separated by a channel of 10 micron, were thermally evaporated on the glass substrate using a shadowmask. Evaporation was conducted with a rate of 5×10^{-3}-1.5×10^{-1} nm/sec, and in a base pressure of 4.5×10^{-7} torr while the growth pressure was varied between 7×10^{-7}-2×10^{-6} torr. The above mentioned process was carried out in a class 10000 cleanroom. Then, the substrate was placed in a Petri dish and its surface was silanised with a few droplets hexamethyldisilazane (HMDS) over a 12 hour period to form a self-assembled hydrophobic surface layer. Au/dodecanethiol CSNPs with a core diameter of 4 nm were sourced from PlasmaChem GmbH (Germany) [18], and were spread from 2 mg/mL chloroform solution onto the water surface of a Langmuir trough. We recorded the surface pressure – area isotherm, Figure 1a. This shows that the gold nanoparticles form a condensed Langmuir film which is stable up to a surface pressure of ~ 20 $mN.m^{-1}$ at which point it collapses. Below or at 20 $mN.m^{-1}$, the area occupied by each nanoparticle corresponds well to the expected cross-sectional area of the nanoparticle, indicating that the layer is monomolecular. We used Langmuir–Schäfer printing [19], where the substrate is lowered with its surface plane parallel to the water surface to gently touch and pick up an Au CSNP monolayer at 18 $mN.m^{-1}$. The process was repeated 4 more times to fabricate multilayer assemblies consisting of five layers.

The resulting films were imaged using tapping mode AFM. This was carried out using a Dimension 3100 AFM with a NanoScope IIIa controller and a Basic extender. RTESPA cantilevers with a nominal spring constant of 40 N/m were driven just below their first resonance (~300 kHz) with an amplitude of approximately 50 nm. Scans were taken with an amplitude setpoint of approximately 90% at a line frequency of 1-2 Hz. All measurements were carried out in air.

Representative images of the film surface are shown in Figure 1 (b,c). The film shows densely packed cores with a measured diameter of approximately 5 nm. Domains of hexagonal close-packing may be seen (dotted box, Figure 1(b), however these domains

typically extend for only a few tens of nanometres. It is also confirmed that the size of the nanoparticles is 4nm, as quoted by the supplier [18].

2.2. Solvents: n-hexane, n-decane, cyclohexane, p-xylene, tuolene, ethanol, and methanol were sourced from Sigma-Aldrich, choloroform, acetone, and isopropanol (IPA) from Fisher Scientific. Apart from n-decane which was anhydrous grade, all solvents were HPLC grade. A sample of a "Premium Unleaded 95 Octane Fuel" was acquired from Total petrol station, Sheffield, UK. Relevant physicochemical properties of solvents are summarised in table 1.

2.3. Vapour Sensing Tests: We conducted qualitative and quantitative exposure tests to investigate the selectivity and sensitivity of our Au CSNP films. The first qualitative test was placing a cotton bud soaked with solvent near the sample (> 1 cm distance). It is worthy mentioned that water vapour exposure test was a slightly different as we heated about 50 ml of water in a basin crystallising up to 65 ^{o}C, and after that it was placed near the sample inside a grounded Faraday cage and then monitored for 5 min. The other qualitative test was conducted by placing the sample and a small Petri dish filled with solvent inside a closed Teflon- lined exposure chamber with electric feed-throughs. This will be referred to as 'headspace' odour exposure. It is worth noting that the odour atmosphere builds up slowly towards saturation and time required to reach saturation varies between solvents.

Quantitative odour exposures were conducted using a vapour delivery system adapted from [26]. We used two Tylan FC-260 mass flow controllers TO control the flow of dry nitrogen along two separate paths, and several one-way valves to prevent backflow. The first path carries pure N_2, the second bubbles N_2 through liquid analyte kept in a small glass container with a sparger (Mobile Phase Sparger Filter, 20μm porosity, bought from Thames Restek Limited, UK). The N_2 flow is driven through the sparger to form tiny bubbles that saturate with solvent vapour as they rise. Saturated vapour then proceeds through a small settlement tank, where floating droplets will condense, towards a mixing point where it is diluted with pure N_2 according to the mass flow controller settings, and is then piped into a small (~8×10^2 cm^3), Teflon-lined exposure chamber that holds the

Au-CSNP film under test. The film is connected to a resistance measurement circuit via electric feed-throughs.

2.4. Resistance Measurement: Au CSNP films display high resistance in the order of GΩ, which requires sensitive measurement. We used the circuit shown in Figure 2(a). The sample, R_S, was driven by a sine input voltage (±1 Volt applied to a 10 μm channel, thus E ≤ 10 kV/cm) with a frequency of 0.2 Hz; a low frequency was chosen to minimise parasitic capacitive currents. The resulting current was driven into the virtual ground of a current / voltage (I/V) converter, realised with a high input impedance operational amplifier (type AD822 with 1.5V supply voltage) and a 100 MΩ feedback resistor (R_f). The circuit was protected from noise interference by a grounded Faraday cage; similarly the exposure chamber was grounded to double as Faraday cage for the sample. Drive voltage (V_{in}) and I/V converter output voltage (V_{out}) were displayed on an oscilloscope screen, see Figure 2b for examples. In all cases, V_{out} was also sinusoidal and in phase with V_{in}, confirming ohmic behaviour of our devices, as the suggested by eq. 1. Ohmic behaviour is shown more clearly in Figure 2c.

Sample resistance R_s is calculated using eq. (1.2):

$$R_S = \frac{V_{in}}{V_{out}} R_f \qquad (1.2)$$

For maximum accuracy, both V_{in} and V_{out} were taken at their maxima. We tested our setup using a 1 GΩ dummy resistor and found (1.00 ± 0.01) GΩ, indicating an error margin of 1%. As a control experiment, we also tested a substrate with Au contacts, but without deposited CSNP film. We found no measurable V_{out} other than a noise floor, from which we can infer a lower limit of at least 100 GΩ for the resistance of blank substrates.

3. Results and discussion

Response of Au CSNP films under qualitative odour exposure (cotton bud) to a variety of solvents is shown in Figure 3, where the relative change in resistance, $\Delta R/R$, is plotted *vs.* Hildebrand parameter and H- bonding strength. Qualitative results agree with the expectation that dodecanethiol core/shell nanoparticle films swell most in odours that are similar to dodecane, with a similarly low Hildebrand solubility parameter (δ), and weak hydrogen- bonding strength, e.g. hexane, decane, toluene, and petrol. However, response is weak ($\leq$ 5 % resistance change) under polar or hydrogen- bonding odours (IPA, acetone, ethanol, methanol, and water). While we cannot precisely quantify odour concentrations with a qualitative test, the strong response to decane is particularly remarkable, as it has a relatively low saturated vapour pressure. Thus, Au-dodecanethiol CSNP films make sensors for explosive alkane and aromatic odours, or their mixtures like petrol, that are robust against interferants such as alcohols, ketones, or humidity (water vapour). Also, we observe rapid recovery of the original resistance, within 30 to 90 seconds and to immeasurably small tolerance, when the bud is removed. As a physical rather than chemical interaction, swelling is rapidly and completely reversible.

A small increase in the resistance was observed when exposing our CSNP films to water vapour. A similar response to water vapour at low humidity was reported for octanethiolate CSNP [27].

The sensors described here work at ambient temperature, without heating. We find film resistance is largely independent of temperature hence changes in temperature will not be misinterpreted as odour exposure, or sensor failure, Figure 3(b). This is a significant advantage of core/shell nanoparticle films over organic semiconductor-based sensors, wherein charge transport is dominated by thermally activated tunnelling [28], and film resistance strongly depends on temperature.

For a more quantitative assessment of sensitivity and recovery, we have exposed films to odours of decane and hexane, Figure 4. We observe a slow increase of resistance over time, which reflects the slow build- up of odour inside the chamber. However, recovery is rapid when the chamber is opened to atmosphere, and the solvent reservoir is removed. (see Figures 2b). As odour atmosphere approaches saturation, $\Delta R/R$ increases 19 fold for hexane (saturated vapour pressure of ~174800 ppm), and about 5 fold for decane

(saturated vapour pressure ~1500 ppm). This indicates highly sensitive response to low levels of decane odours, in particular.

To explore the sensitivity limit of our films to decane, we have subjected films to exposure/recovery cycles of dilute decane odours, generated with the bubbler / mixer setup described above. We began with 1% sat. vapour / 99% pure nitrogen, corresponding to 15 ppm decane, and increased odour concentration in several steps. Results are shown in Figure 5 (a). We find that core/shell nanoparticle film resistance clearly and rapidly responds to decane odours with concentrations as low as 15 ppm, well below the LEL of 8000 ppm. Response is quick, levels off to a flat plateau, and the sensor recovers rapidly back to its initial value under plain N_2 purge. Response plateau scales approximately linearly with odour concentration at low concentrations, as depicted in Figure 5 (b). When approaching saturation, response appears to increase more than linearly, however, this is based on a single data point taken from the previous 'headspace' experiment, because we cannot exceed 50% saturation due to the limitation of our bubbler.

4. Summary and Conclusions

We deposit dense, ordered, thin films of Au- dodecanethiol core/shell nanoparticles by the Langmuir- Schäfer (LS) printing method. Resulting films display ohmic electric behaviour with high resistance, consistent with carrier transport by site- to- site tunnelling. We find that films respond selectively and sensitively under exposure to alkane odours. Response is in the form of a rapid increase of resistance, which we explain as the result of swelling, since conductivity decrease exponentially with distance for tunnelling transport. Response is strongest for alkane odours where the alkane chain is similar in length to the dodecane shell. For decane odours, we find a response to concentrations as low as 15 ppm, which is about 600 times below the lower explosive limit. Response is weaker, but still significant, to aromatic odours (e.g. Toluene, Xylene), while polar and/or hydrogen- bonding odours (e.g. alcohols, ketones) are almost rejected. Humidity seems to have no or little effect on the resistance ($\leq$ 5 % increase). Further, resistance depends weakly on temperature, and recovers rapidly and completely to its

original value within the error margin of measurement. In summary, we have demonstrated sensitive and selective sensors to alkane odours well below their lower explosive limit, which reject common interferants, operate at ambient temperature, and fully recover after exposure. Future work will address similarly processed nanoparticle films with different sidechains, e.g. shorter sidechains to be more responsive to light alkanes, sidechains containing aromatic units for aromatic odours, and sidechains containing unsaturated carbon bonds for ethylene.

Acknowledgements

H Al Qahtani acknowledges the sponsorship of King Saud University. L Hague and N Mullen thank the UK ‘Engineering and Physical Sciences Research Council’ (EPSRC) for the provision of a doctoral training account (LH), and a postdoctoral fellowship (NM), respectively. D Puzzovio thanks the European Commission for the provision of an ‘Experienced Researcher’ Marie Curie fellowship under the ‘FlexSmell’ Initial Training Network. The authors thank Dr J Hobbs of Dept. of Physics and Astronomy, University of Sheffield, for access to his AFM facilities.

References

[1] Lorna Gordon, "Fifteen people injured in Salford gas explosion", in *BBC News* (http://www.bbc.co.uk/news/uk-11676314, 2010).

[2] "Buncefield tank 'was overflowing'", in *BBC News* (http://news.bbc.co.uk/1/hi/uk/4752819.stm, 2006).

[3] "Deaths as fire hits Saudi gas plant", in *Aljazeera.net* (http://english.aljazeera.net/news/middleeast/2007/11/200852512551982490 8.html, 2007).

[4] Adam Gabbatt, "New Zealand mine rescuers prepare for deaths", in *The Guardian* (http://www.guardian.co.uk/world/2010/nov/22/new-zeland-rescuers-prepare-death?intcmp=239, 2010).

[5] D. Koziej, N. Barsan, V. Hoffmann, J. Szuber, and U. Weimar, "Complementary phenomenological and spectroscopic studies of propane sensing with tin dioxide based sensors," Sensors and Actuators B-Chemical **108** (1-2), 75-83 (2005).

[6] S. Chakraborty, A. Sen, and H. S. Maiti, "Selective detection of methane and butane by temperature modulation in iron doped tin oxide sensors," Sensors and Actuators B-Chemical **115** (2), 610-613 (2006).

[7] M. C. Carotta, V. Guidi, G. Martinelli, M. Nagliati, D. Puzzovio, and D. Vecchi, "Sensing of volatile alkanes by metal-oxide semiconductors," Sensors and Actuators B-Chemical **130** (1), 497-501 (2008).

[8] M. C. Carotta, A. Cervi, A. Giberti, V. Guidi, C. Malagu, G. Martinelli, and D. Puzzovio, "Metal-oxide solid solutions for light alkane sensing," Sensors and Actuators B-Chemical **133** (2), 516-520 (2008).

[9] M. C. Carotta, A. Cervi, A. Giberti, V. Guidi, C. Malagu, G. Martinelli, and D. Puzzovio, "Ethanol interference in light alkane sensing by metal-oxide solid solutions," Sensors and Actuators B-Chemical **136** (2), 405-409 (2009).

[10] H. Wohltjen and A. Snow, “Colloidal Metal-Insulator-Metal Ensemble Chemiresistor Sensor,” Anal. Chem., 70, 2856-2859.

[11] H. Ahn, A. Chandekar, B. Kang, C. Sung, and J. E. Whitten, "Electrical conductivity and vapor-sensing properties of omega-(3-thienyl)alkanethiol-

protected gold nanoparticle films," Chemistry of Materials **16** (17), 3274-3278 (2004).

[12] E. Garcia-Berrios, T. Gao, M. Woodka, S. Maldonado, B. Brunschwig, M. Ellsworth, N. Lewis, "Response versus chain length of alkanethiol-capped Au nanoparticles chemiresistive chemical vapor sensors," J. Phys. Chem. C 114, 21914-21920 (2010).

[13] S. Y. Heriot, H. L. Zhang, S. D. Evans, and T. H. Richardson, "Multilayers of 4-methylbenzenethiol functionalized gold nanoparticles fabricated by Langmuir-Blodgett and Langmuir-Schaefer deposition," Colloids and Surfaces a-Physicochemical and Engineering Aspects **278** (1-3), 98-105 (2006).

[14] S. D. Evans, S. R. Johnson, Y. L. Cheng and T. Shen, "Vapour sensing using hybrid organic–inorganic nanostructured materials," J. Mater. Chem., 10, 183-188 (2000).

[15] M. D. Hanwell, S. Y. Heriot, T. H. Richardson, N. Cowlam, and I. M. Ross, "Gas and vapour sensing characteristics of Langmuir-Schaeffer thiol encapsulated gold nanoparticle thin films," Colloids and Surfaces a-Physicochemical and Engineering Aspects **284**, 379-383 (2006).

[16] R. Terrill, T. A. Postlethwaite, C. Chen, C. Poon, A. Terzis, A. Chen, J. Hutchison, M. Clark, G. Wignall, J. Londono, R. Superfine, M. Falvo, C. Johnson Jr., E. Samlski, and R. Murry, "Monolayers in three dimensions:NMR, SAXS, thermal, and electron hopping studies of alkanethiol stabilised gold clusters," J. Am. Chem. Soc. 117, 12537-12548 (1995).

[17] A. Zabet-Khosousi and A. Dhirani, "Charge Transport in Nanoparticle Assemblies," Chem. Rev. 108, 4072-4124 (2008).

[18] http://www.plasmachem.com

[19] M. C. Petty, "*An Introduction to Langmuir-Blodgett Films*," Cambridge University Press, Cambridge, 1996.

[20] E. A. Grulke, "Solubility parameter values", in *Polymer Handbook*, edited by J. Brandrup and E. H. Immergut (John Wiley & Sons, New York, 1989).

[21] "Polymer Solutions: Solvents and Solubility Parameters", in *Sigma-Aldrich.com* (http://www.sigmaaldrich.com/etc/medialib/docs/Aldrich/General_Information/polymer_solutions.Par.0001.File.tmp/polymer_solutions.pdf).

[22] E. S. Tarleton, J. P. Robinson, and J. S. Low, "Nanofiltratioon: A technology for selective solute removal from fuels and solvents," Chemical Engineering Research & Design **87** (3A), 271-279 (2009).

[23] "Chemical and Other Safety Information", The Physical and Theoretical Chemistry Laboratory, Oxford University (http://msds.chem.ox.ac.uk).

[24] R. D. Chirico, A. Nguyen, W. V. Steele, and M. M. Strube, " Vapor pressure of n-alkanes revisited. New high-precision vapor pressure data on n-decane, n-eicosane, and n-Octacosanet," Journal of Chemical and Engineering Data **34** (2), 149-156 (1989).

[25] "Humidity and water vapour pressure calculator", (http://www.see.ed.ac.uk/~jwp/newWork/Chemeng/Chemeng/water.html).

[26] S. Brittle, T. H. Richardson, A. D. F. Dunbar, S. Turega, and C. A. Hunter, "Alkylamine sensing using Langmuir-Blodgett films of n-alkyl-N-phenylamide-substituted zinc porphyrins," J. Phys. Chem. B **112** (36), 11278-11283 (2008).

[27] P. Pang, Z. Guo, and Q. Cai, "Humidity effect on the monolayer-protected gold nanoparticles coated chemiresistor sensor for VOCs analysis," Talanta 65, 1343-1348 (2005).

[28] W. F. Pasveer, J. Cottaar, C. Tanase, R. Coehoorn, P. A. Bobbert, P. W. M. Blom, D. M. de Leeuw, and M. A. J. Michels, "Unified description of charge-carrier mobilities in disordered semiconducting polymers," Physical Review Letters **94** (2005).

Figure Captions

Figure 1: (a) Langmuir isotherm of core/shell nanoparticles. This was recorded using Nima 611D Standard Trough run by Nima software. Inset: Photo of resulting device. Au contacts are 2 mm wide, and separated by a 10 μm gap. (b) Tapping mode AFM height image rendered in 3d. Colour scale 5 nm, scale bar 50 nm. (c) Simultaneously acquired tapping mode phase image. The white dotted box denotes a domain of hexagonally close packed nanoparticles. Colour scale 12°, scale bar 50 nm.

Figure 2: (a) Scheme of our drive and measurement circuit. The sample is denoted by R_s; an I/V converter is realised by the operational amplifier and feedback resistor, R_f. (b) Oscilloscope screenshots, showing Vin (orange, 1V/div), and Vout (blue, 50mV/div) of Au CSNP films prior to exposure, during exposure to 1500 ppm of decane odour, and during recovery. Output is shown inverted to account for the inversion intrinsic to the I/V converter. Output is of the same (sinusoidal) form as input, and in phase. Under exposure, Vout is significantly reduced, which indicates increased film resistance due to swelling. Recovery is rapid and the screen looks almost identical to 'before sensing' within 1 minute. (c) Current/Voltage characteristics of the same film before sensing, and after full recovery. The plot is constructed from I/V converter data taken from screenshots as in 2b, and plotting output vs. input directly, eliminating the time base. Characteristics are linear, confirming ohmic behaviour.

Figure 3: (a) Response of Au CSNP films to odours of different Hildebrand parameters and hydrogen bonding strength. (b) the change in resistance of CSNP films upon varying the temperature between 22 and 50 ^{o}C.

Figure 4: 'Headspace' exposures to decane and hexane. The recovery starting point in each case is indicated by "Off". In each case, the sample returned to its original value.

Figure 5: (a) Resistance change under exposure/recovery cycles, beginning with 15 ppm decane odour. (b) ΔR/R plateau vs. vapour pressure. The value for 1500 ppm is taken from previous 'headspace' exposure.

Table Captions

Table 1: Properties of solvents. Column 2: Hildebrand parameter (δ), quantifying cohesive energy density. In round brackets, hydrogen bonding strength (poor / medium / strong). Column 3: Saturated vapour pressure, in ppm, at 20 ^{o}C. Column 4: Lower explosive limit, in ppm. Angled brackets, source of data.

Figure 1

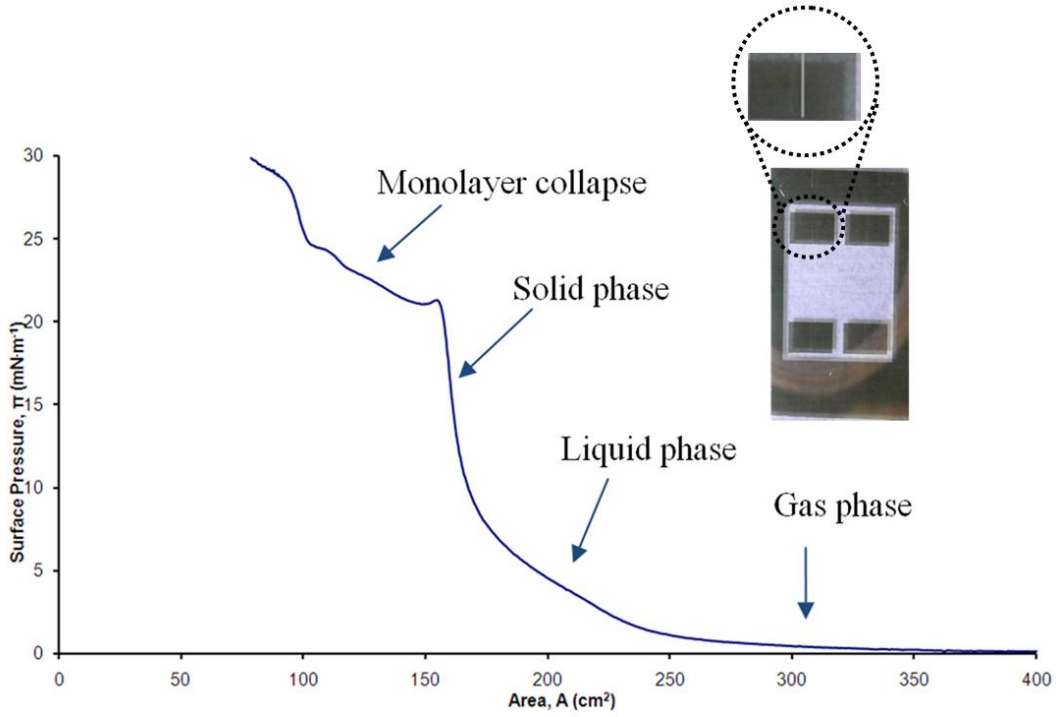
Monolayer collapse
Solid phase
Liquid phase
Gas phase
Surface Pressure, π (mN·m⁻¹)
Area, A (cm²)
0
5
10
15
20
25
30
0
50
100
150
200
250
300
350
400

(a)

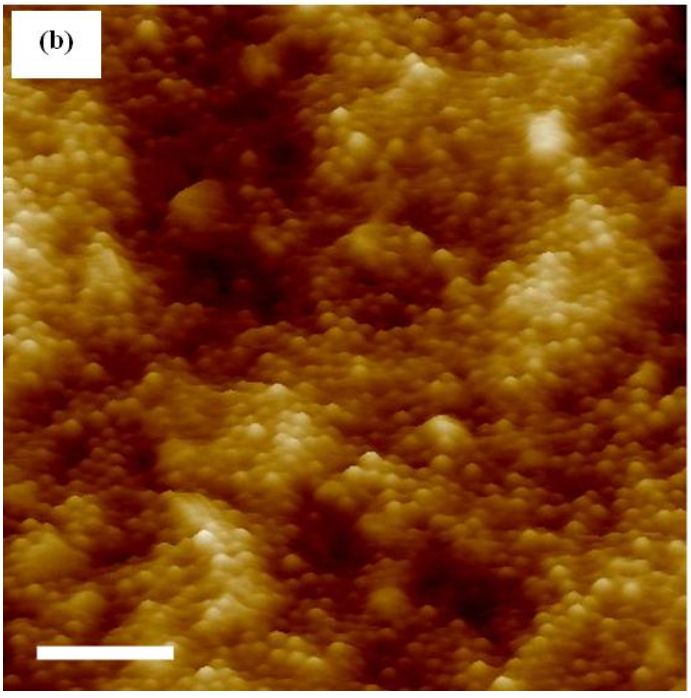
(b)

(b)

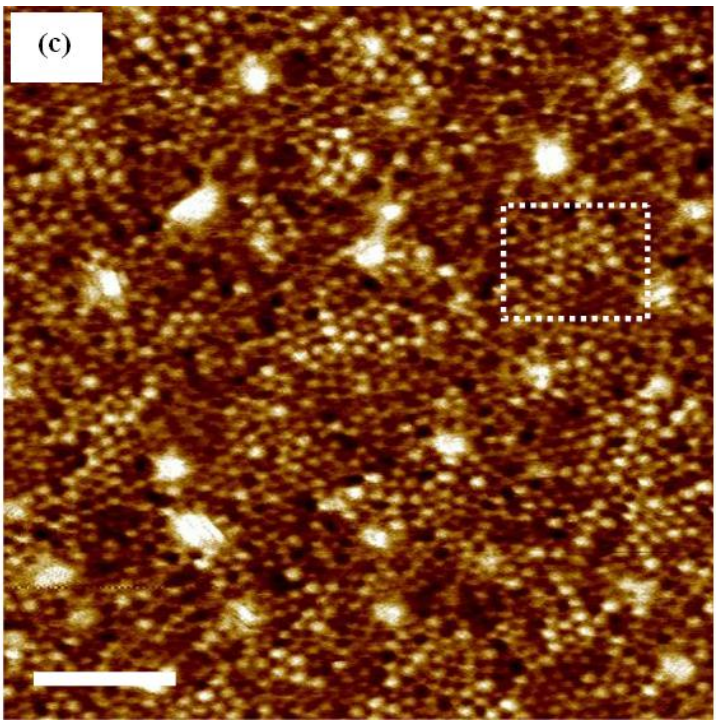

(c)

Figure 2

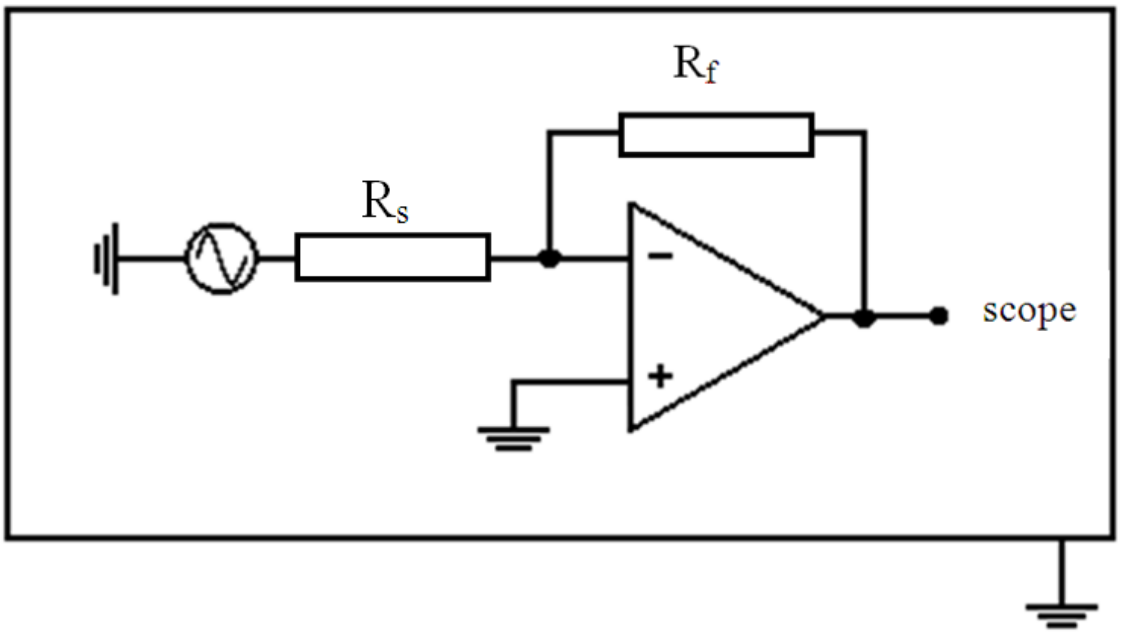
R_f
R_s
scope

(a)

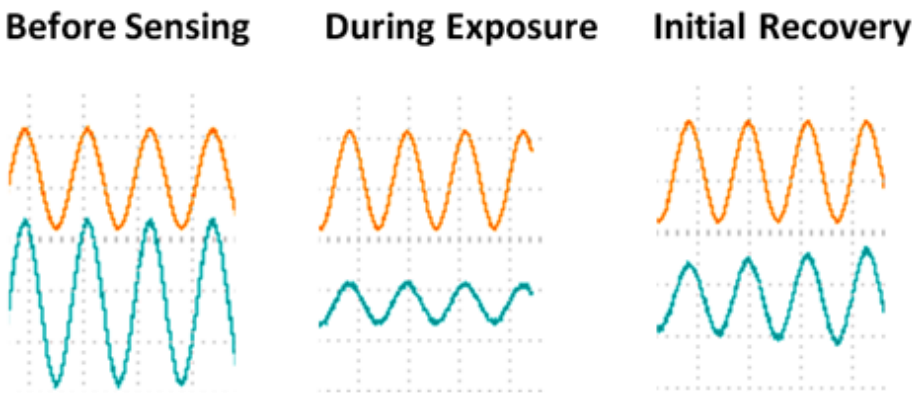
Before Sensing
During Exposure
Initial Recovery

(b)

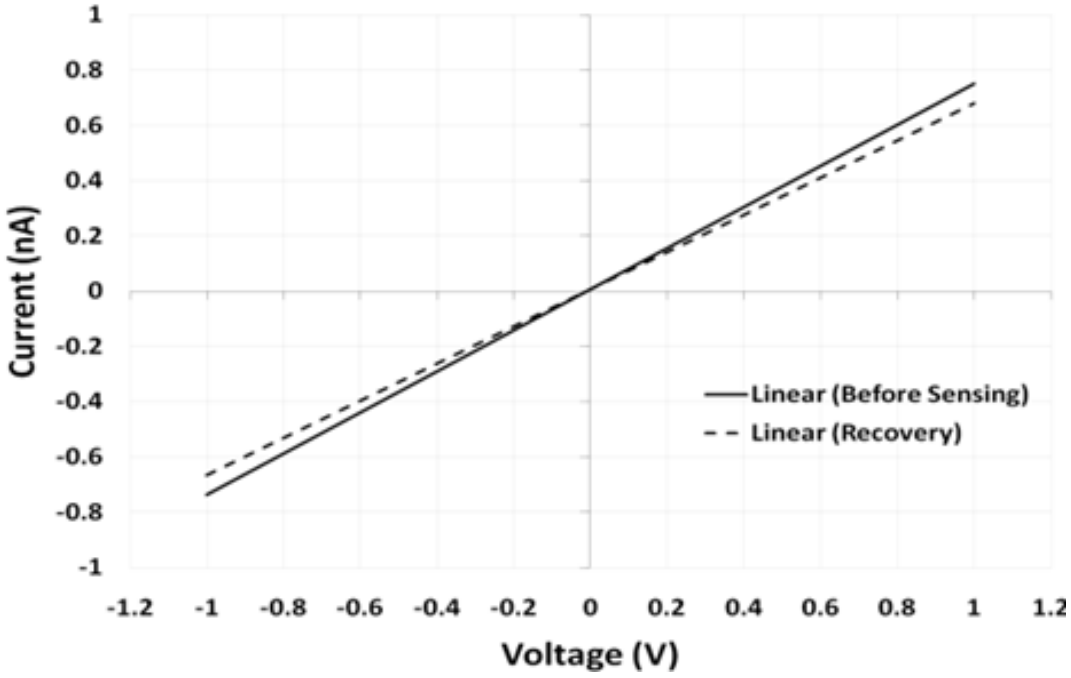
Current (nA)
Voltage (V)
Linear (Before Sensing)
Linear (Recovery)
1
0.8
0.6
0.4
0.2
0
-0.2
-0.4
-0.6
-0.8
-1
-1.2
-1
-0.8
-0.6
-0.4
-0.2
0
0.2
0.4
0.6
0.8
1
1.2

(c)

Figure 3

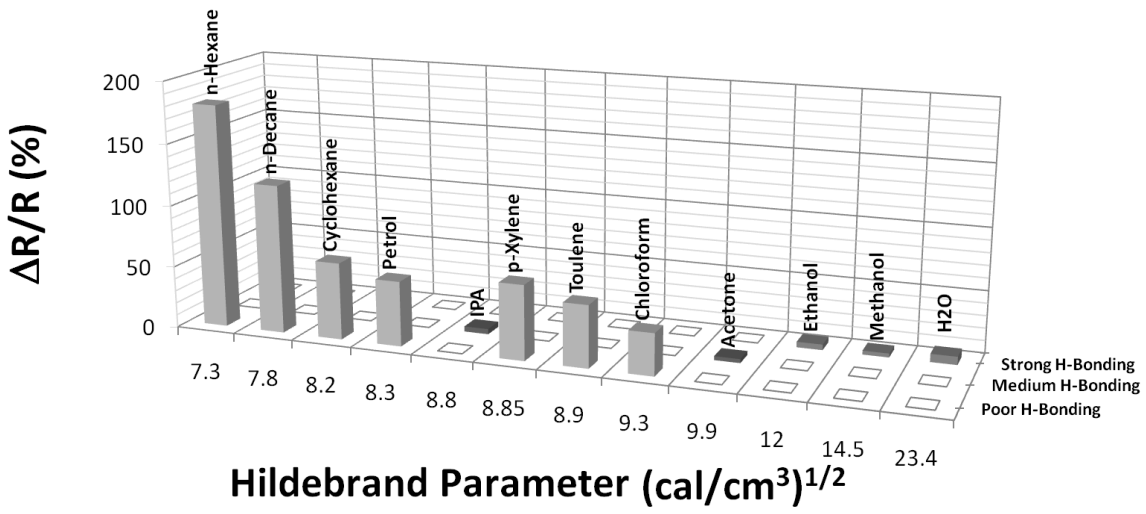
ΔR/R (%)
200
150
100
50
0
n-Hexane
n-Decane
Cyclohexane
Petrol
IPA
p-Xylene
Toulene
Chloroform
Acetone
Ethanol
Methanol
H2O
7.3
7.8
8.2
8.3
8.8
8.85
8.9
9.3
9.9
12
14.5
23.4
Strong H-Bonding
Medium H-Bonding
Poor H-Bonding
Hildebrand Parameter (cal/cm3)1/2

(a)

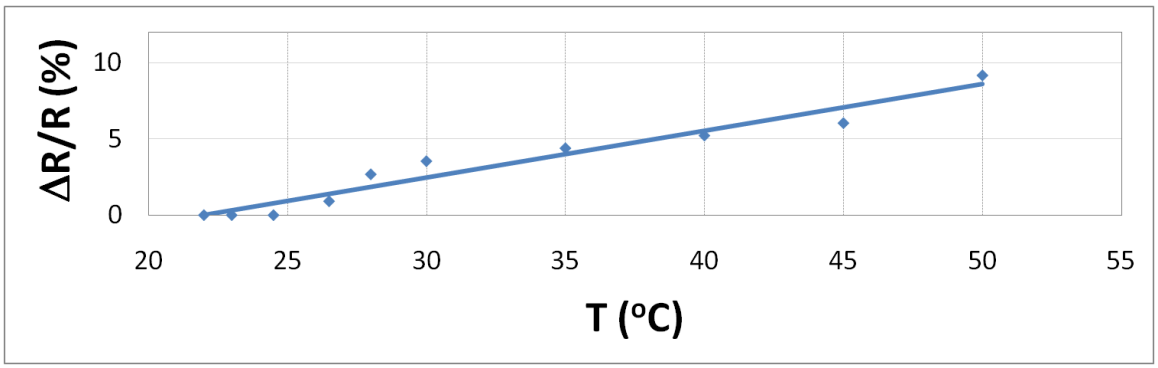
ΔR/R (%)
10
5
0
20
25
30
35
40
45
50
55
T (°C)

(b)

Figure 4

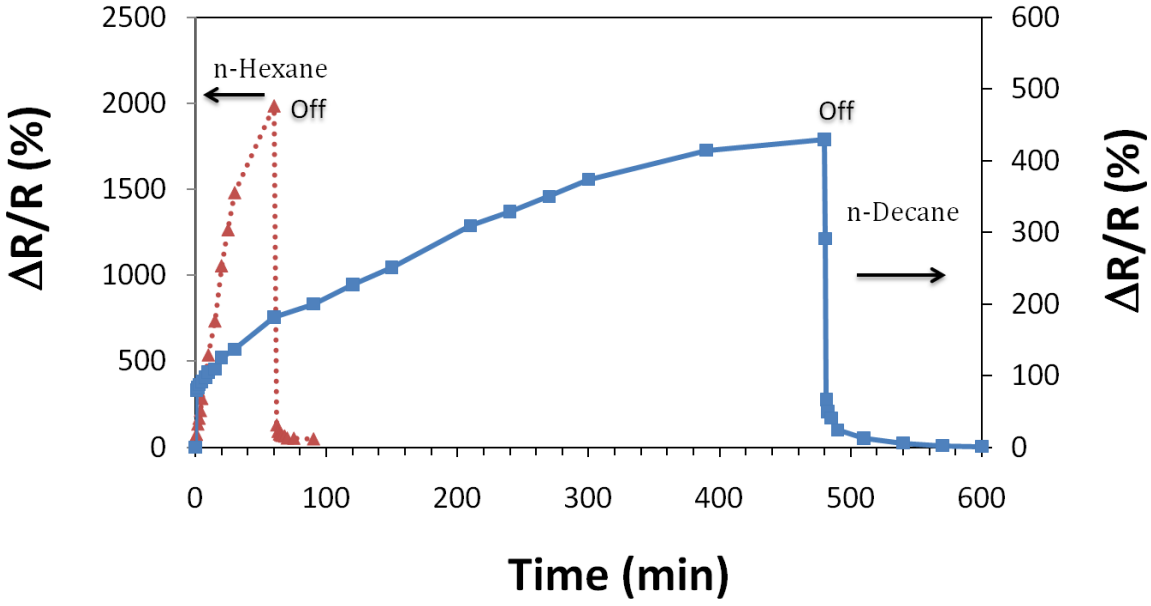
2500
2000
1500
1000
500
0
ΔR/R (%)
n-Hexane
Off
Off
n-Decane
600
500
400
300
200
100
0
ΔR/R (%)
0
100
200
300
400
500
600
Time (min)

Figure 5:

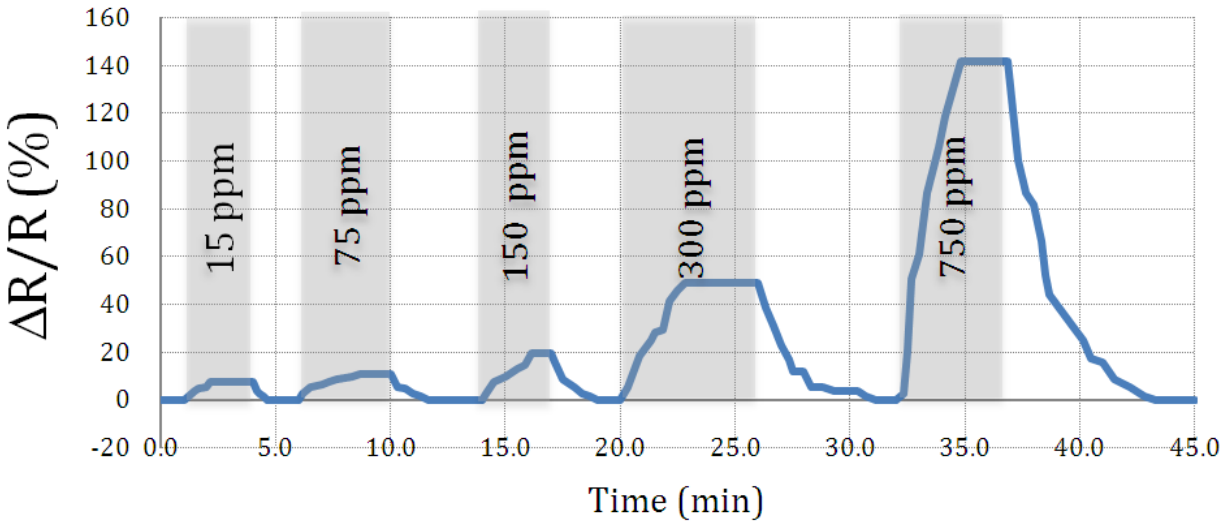
ΔR/R (%)
160
140
120
100
80
60
40
20
0
-20
0.0
5.0
10.0
15.0
20.0
25.0
30.0
35.0
40.0
45.0
15 ppm
75 ppm
150 ppm
300 ppm
750 ppm
Time (min)

(a)

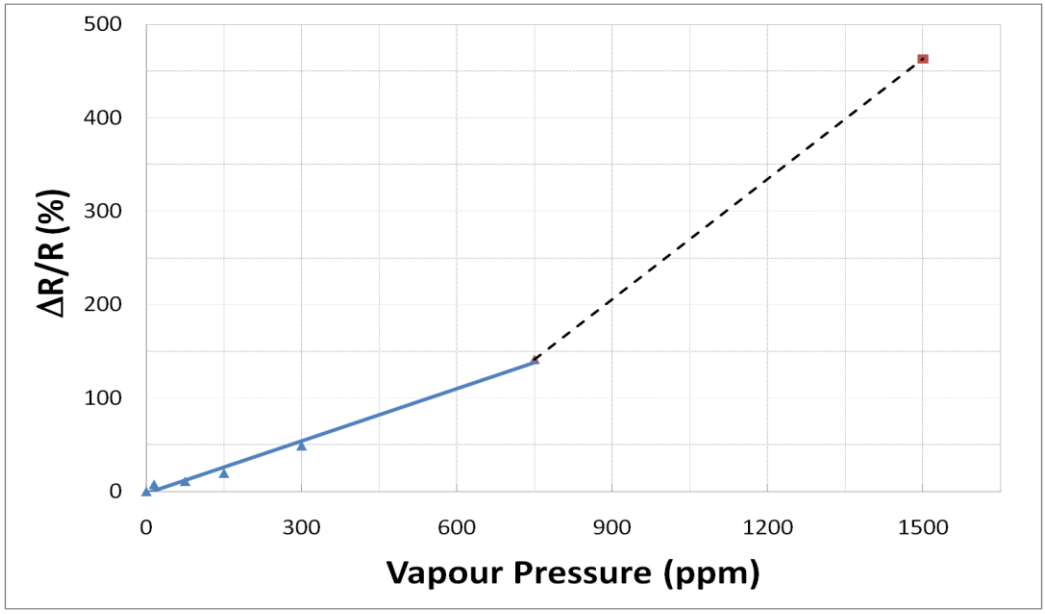
ΔR/R (%)
500
400
300
200
100
0
0
300
600
900
1200
1500
Vapour Pressure (ppm)

(b)